Available online at www.CivileJournal.org

Civil Engineering Journal

(E-ISSN: 2476-3055; ISSN: 2676-6957)

Vol. 11, No. 07, July, 2025

Alternative Method for Determining Manning's Roughness Coefficient Using Two-Point Velocity in Equilibrium and Nonequilibrium Sediment Transport

Miskar Maini [1, 2], Bambang A. Kironoto [1*], Adam P. Rahardjo [1], Istiarto [1]

[1] *Department of Civil and Environmental Engineering, Faculty of Engineering, Universitas Gadjah Mada, Yogyakarta, Indonesia.*

[2] *Department of Civil Engineering, Faculty of Infrastructure and Regional Technology, Institut Teknologi Sumatera, Lampung Selatan, Indonesia.*

Received 29 November 2024; Revised 15 May 2025; Accepted 22 May 2025; Published 01 July 2025

Abstract

Understanding flow resistance equations, such as Manning's roughness equation, is essential for river design and improvement. Estimating Manning's roughness coefficient becomes more complicated when sediment transport is involved. This study takes an alternative approach by using velocity profiles to examine how sediment transport affects Manning's roughness coefficient. To achieve this goal, 1200 velocity profiles with sediment-feeding (SF) and non-sediment-feeding (NSF) flows are evaluated to determine the (composite) Manning's roughness coefficient. Sediment-feeding flows describe sediment flow under equilibrium conditions, whereas non-sediment-feeding flows represent sediment flow under nonequilibrium conditions. A Sontek 16-MHz Acoustic Doppler Velocimeter is used to measure the velocity (and turbulence) profiles. In addition to the present data, 225 secondary velocity profile data sets are analyzed in this study. The research findings indicate that the composite Manning's roughness coefficient n_{co} can be determined from Manning's roughness coefficient $n_{z/B}$ at z/B in the transversal direction, using two points of the velocity profile at $y/H = 0.2$ and 0.4 in the vertical direction. The differences in the velocity profile shape (u/U) due to sediment feeding, particularly in inner regions ($y/H \leq 0.2$), affect the value of $n_{z/B}$. n_{co} for sediment-feeding flows are generally higher than the cross-section Manning roughness coefficient n. As n_{co} (based on $n_{z/B}$) is based on the velocity profile, the n_{co} values change with sediment transport. Meanwhile, the n values remain unchanged because the equation variables cannot detect the presence of sediment transport. For non-sediment-feeding flow, the differences in n_{co} with n are 14.80% for a fixed bed (FB) and 18.17% for a movable bed (MB). The differences are even more pronounced for sediment-feeding flow at 33.01% for a fixed bed and 36.52% for a movable bed. The point where $n_{z/B}/n_{co} = 1$ occurs at $z/B = 0.2$ from the channel sidewall. This suggests that $n_{z/B}$, measured at $z/B = 0.2$ from the channel sidewall, provides a good representation of n_{co} for the section.

Keywords: Manning Roughness Coefficient; Velocity Profile; Sediment Feeding.

1. Introduction

Manning's roughness coefficient (n) is a crucial parameter in hydraulic studies. It quantifies flow resistance along channel surfaces and plays a key role in the planning and analysis of water resource infrastructures, including rivers, canals, and drainage systems [1, 2]. Conventionally, Manning's roughness coefficient is determined using empirical tables or subjective assessments based on channel characteristics [3, 4]. However, these methods often introduce

* Corresponding author: kironoto@ugm.ac.id

http://dx.doi.org/10.28991/CEJ-2025-011-07-02

uncertainties and inconsistencies, particularly in dynamic sediment transport conditions. Given these challenges, a deeper understanding of how sediment transport influences Manning's roughness coefficient is essential for improving the accuracy of hydraulic modeling.

One of the key factors affecting Manning's roughness is sediment transport, which can occur in either equilibrium (where sediment inflow and outflow are balanced) or nonequilibrium conditions (where discrepancies exist between sediment entering and leaving the section). These imbalances can cause significant changes in riverbed configuration, such as degradation or aggradation, ultimately affecting Manning's roughness coefficient. To better understand these interactions, several studies have examined how sediment transport influences flow resistance and bed roughness.

For instance, Rad et al. (2025) [5] demonstrated that different flow rates, categorized as low and high flow, significantly influence Manning's roughness coefficient. Furthermore, in sediment-laden flow conditions, Manning's roughness varies because of changes in flow velocity, sediment distribution, and channel geometry characteristics [6, 7]. Meanwhile, Zhang et al. (2010) [8] found that under sediment-laden flow conditions with a maximum concentration of 974 kg/m³, Manning's roughness coefficient increased by 51.27% compared with that of a sediment-free flow. Similarly, Maini et al. (2024) [7] showed that sediment-feeding flow led to a 19% increase in Manning's roughness coefficient compared with non-sediment-feeding flow using 0.92-mm sand sediment. Additional research has confirmed that bedload sediment transport increases the channel bed roughness [9-11] and reduces flow velocity [12, 13]. In turbulent flow regimes with rough channel beds, the logarithmic velocity distribution has been successfully modeled using semiempirical logarithmic law approaches [14, 15]. Still, significant knowledge gaps remain despite these studies, particularly in real-world applications beyond controlled laboratory environments.

Conventional or empirical methods derived from the cross-sectional mean velocity still fail to capture real-time flow variability and dynamic bedform adjustments, which are crucial for accurate hydraulic modeling. Meanwhile, recent literature (2024–2025) has shown advances in measurement techniques, mainly through the application of acoustic sensor technology and numerical models, which enable more precise estimation of Manning's roughness under complex sediment transport conditions. For example, Maini et al. (2024) [7] used acoustic Doppler velocimetry (ADV) to determine Manning's roughness based on velocity measurements at two points ($0.1H$ and $0.2H$), providing a more representative approach to the velocity distribution in sedimented flows. Meanwhile, Zhang et al. (2025) [16] conducted laboratory experiments using numerical models to analyze sediment transport capacity. Furthermore, Hou & Zhang (2025) [17] analyzed a validated numerical model using field measurement data from downstream of the Yellow River. They found that the water depth calculated using the friction correction curve method showed that under flat and static riverbed conditions, the absence of resistance due to sand waves caused low flow resistance.

This study proposes an alternative approach for determining Manning's roughness based on two-point velocity measurements and logarithmic velocity profiles to address the above limitations, particularly those associated with conventional or empirical methods. Unlike conventional or empirical methods, this approach dynamically accounts for real-time flow conditions, bedform changes, and sediment transport, thus improving prediction accuracy. Furthermore, it provides dynamic roughness values that evolve with the flow depth and velocity, enhancing adaptability to unsteady flow conditions. To validate the proposed approach, this study uses laboratory measurement data (for equilibrium and nonequilibrium sediment transport conditions) and field data from constructed irrigation channels and natural rivers.

This article is structured into several key sections. The first section explains the experimental setup and measuring equipment used in the study. The following section develops Manning's roughness values using two-point velocity measurements. The results and discussion section presents the findings along with the data analysis. Finally, this article concludes with the main findings of the analysis.

2. Methodology and Theoretical Background

The stages of this research are illustrated in the flowchart in Figure 1, which depicts the experimental process and analysis of the flow velocity distribution and Manning's roughness coefficient in a laboratory flume. Velocity profile measurements were conducted using an ADV. The quality of the obtained data was evaluated on the basis of the signal-to-noise ratio (SNR) threshold (>15 dB) and correlation level (>70%) to ensure the validity of the measurement results. The experiment included parameter variations such as channel bed roughness, flow discharge, channel bed slope, sediment grain characteristics, and sediment load. The analysis involved calculating average velocities and determining Manning's roughness coefficient using two-point velocity measurements, including variations in the two-point velocity measurement locations.

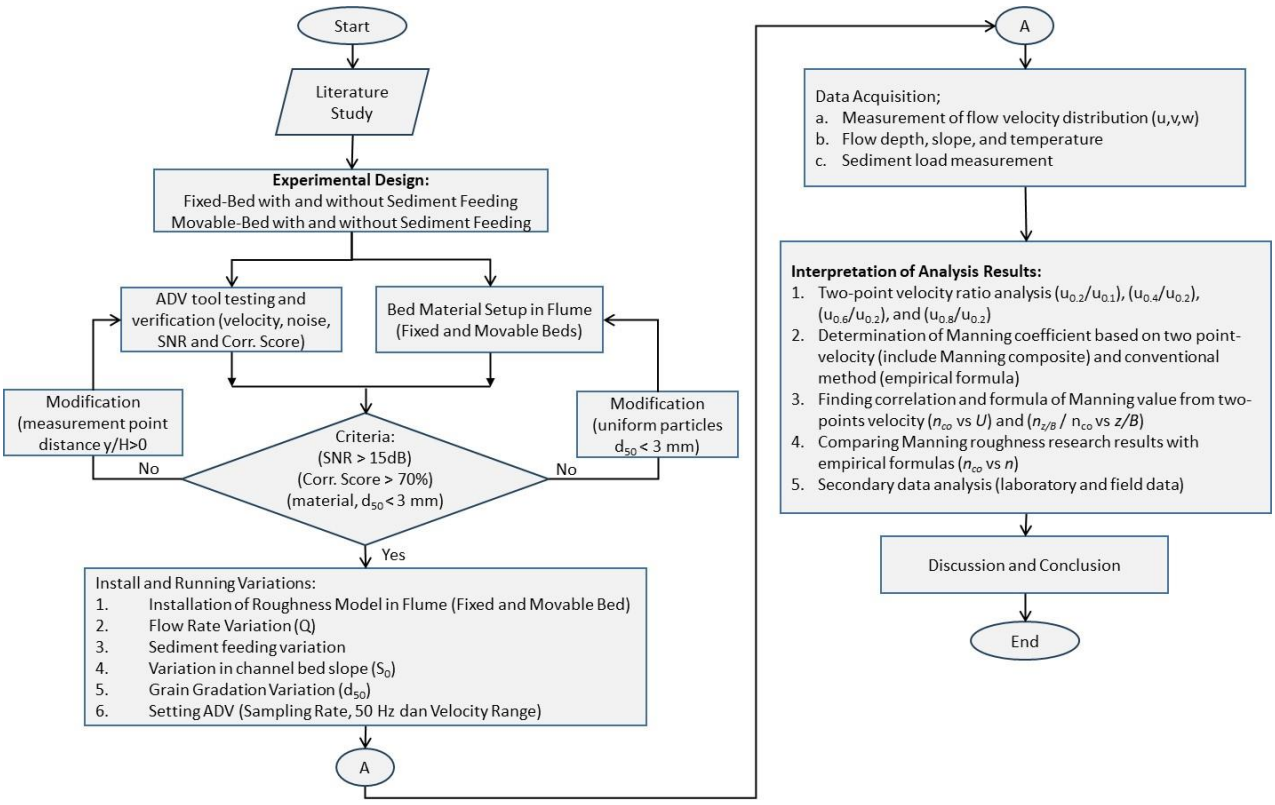

Figure 1. Flow chart of research

2.1. Experimental Set-up and Measuring Equipment

The experiments were conducted at the Hydraulics Laboratory, Department of Civil and Environmental Engineering, Universitas Gadjah Mada, Yogyakarta, Indonesia, using a 10-m-long, 0.6-m-wide, and 0.45-m-high inclined flume. Flow circulation was maintained by a main pump with a capacity of 119 l/s and a secondary pump with a flow rate of 65 l/s, ensuring continuous flow with up to 3% sediment by weight, with a maximum particle size of 3 mm. To prevent the sediment from settling, a hydrocyclone pump was employed to recirculate the sediment from the tank continuously. A schematic of the flume used in this study is shown in Figure 2.

The study investigated two types of bed conditions: a fixed bed and a movable bed. The fixed bed was made of coarse sand glued to a plate, with roughness heights of 1.55 and 1.85 mm, whereas the movable bed consisted of uniform coarse sand with average diameters of 1.55 and 1.85 mm and a thickness of 10 cm. These sediment sizes were chosen considering that the maximum allowable particle size for flowing in the flume system was 3 mm. Additionally, these sediment sizes are commonly found in natural rivers. The flow discharge ranged from 50 to 70 l/s, and three different bed slopes were tested: 0.15%, 0.25%, and 0.35% for sand bed material 1 and 0.20%, 0.30%, and 0.40% for sand bed material 2. Sediments transported in the channel were collected using a sediment trap and recirculated upstream at controlled feeding rates between 0.0049 and 0.0264 kg/s to achieve equilibrium and nonequilibrium sediment transport conditions. The bed surface experienced a reduction of 0.5 to 1.6 cm/hour, depending on the sediment load carried by the flow.

The velocity (and turbulence profiles) were measured using a SONTEK 16-MHz MicroADV Probe with a 99% accuracy rate. Under steady uniform flow conditions, three-dimensional velocity measurements were taken at a sampling frequency of 50 Hz for 60 s, resulting in 3,000 instantaneous velocity data points. Measurements were conducted at two sections: x = 5.6 m (Section 1) and x = 6.6 m (Section 2) from the entrance of the flume, covering half of the cross-section. At each section, five vertical profiles were measured at the following positions: VA = 1/2B, VB = 1/3B, VC = 1/4B, VD = 1/6B, and VE = 1/12B. Each profile consisted of 16 to 32 measurement points, with intervals of 0.2 cm in the inner region ($y/H \leq 0.2$) and 0.5 cm in the outer region ($y/H \geq 0.2$). Data were analyzed if they had an SNR greater than 15 dB and a correlation score above 70%. Because of the ADV limitations, measurements could not be taken within 5 cm of the free surface or within 4.83 cm of the channel sidewall. A sketch illustrating the limitations of the ADV and the vertical measurement positions of velocity in the flume cross-section is provided in Figure 3.

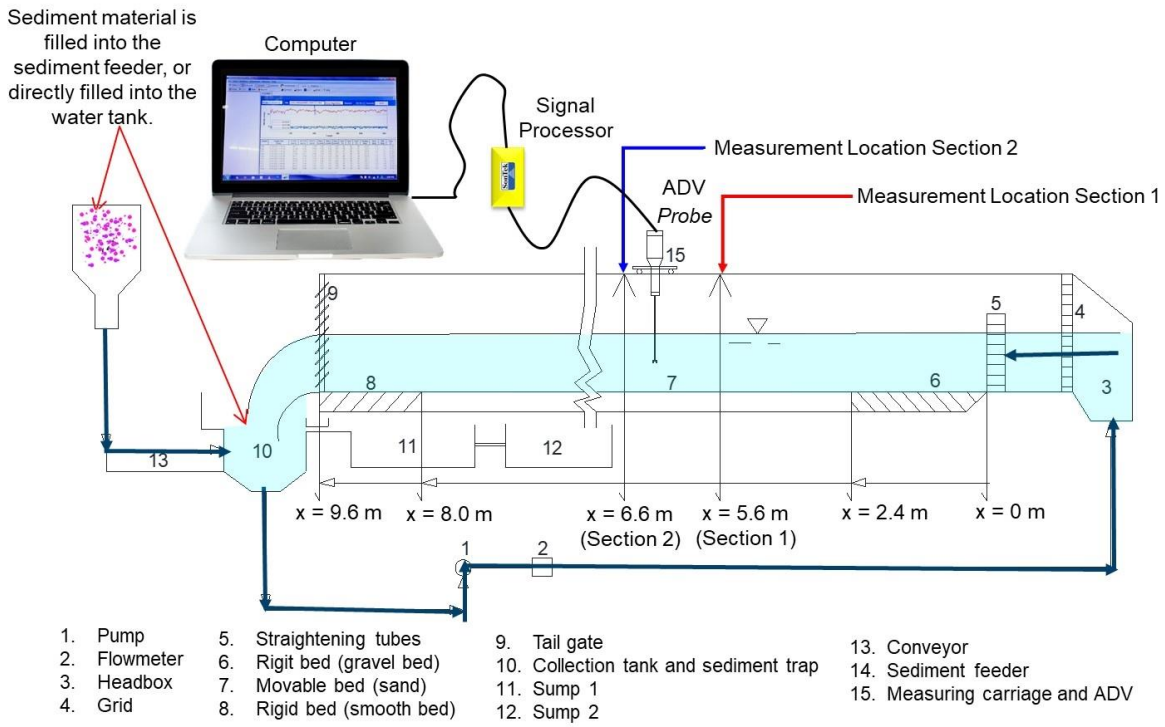

Figure 2. Schematic of flume

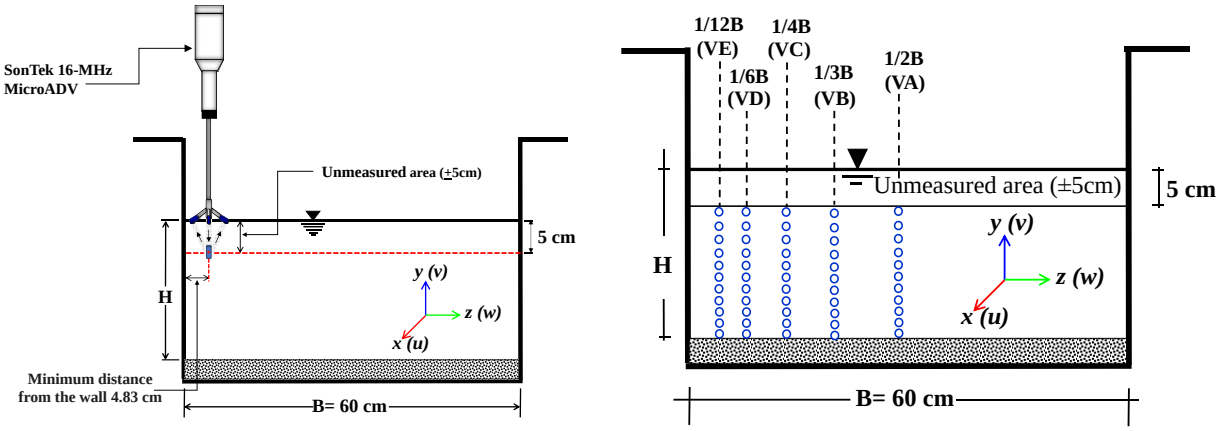

(a) (b)

Figure 3. (a) Sketch of the limitations of ADV in measuring velocity, and (b) vertical measurement positions in the flume cross-section

2.2. Cross-section Manning's Roughness Equation

The cross-section Manning's roughness *n* can be determined using Manning's formula [18]:

$$n = \frac{R^{2/3} S^{1/2}}{U} \quad (1)$$

where *U* is the cross-sectional mean velocity, *R* is the hydraulic radius, and *S* is the energy slope, typically estimated as the slope of the free water surface in uniform flow conditions. The cross-section Manning's roughness coefficient *n* can be determined from the *R* (or flow depth *H*), *U*, and *S* measurement data. However, the accuracy of Manning's roughness coefficient from Equation (1) relies heavily on the precise measurement of the free water surface slope. As this slope is usually very small, even slight errors in the measurement of the water level due to free water surface fluctuations can result in significant inaccuracies in the calculated Manning's roughness coefficient. Furthermore, this equation cannot detect changes in Manning's roughness when sediment transport occurs.

2.3. Velocity Distribution

The velocity distribution profile in open channel flow generally follows a logarithmic pattern, often called the log law. This principle has been essential in hydraulic engineering since it was introduced by Keulegan (1938) [19]. The

similarities in the behavior of velocity distributions in clear water flow and sediment-laden flows demonstrate the usefulness of logarithmic velocity profiles. In this respect, Woo et al. (1988) [20] and van Rijn (1993) [21] formulated a general expression for the logarithmic velocity distribution at various flow depths in smooth and rough flows:

$$u = \frac{u_*}{\kappa} \ln\left(\frac{y}{y_o}\right) \quad (2)$$

where u is the mean point velocity at a distance y from the reference level. The shear velocity (u_*) is calculated using the Clauser method [22-24]. The Karman constant, denoted by κ, has a value of 0.4. The zero-velocity level, where u = 0 at $y = y_o$, also known as the reference level, is denoted as y_o. In the case of a rough boundary, the exact position of the zero-velocity level is uncertain because of its dependence on various factors such as the height, concentration, and gradation of the roughness elements. Some researchers suggest that the reference level can be determined through trial and error so that the universal log law can accurately reproduce the measured velocity profile, especially in the inner region ($y/H \leq 0.2$). Some literature suggests that the reference level is related to the bottom roughness. The reference level, denoted as y_0, is typically positioned between the top and bottom of the surface elements and is measured downward from the average top roughness level [21]. For instance, Einstein & El-Samni (1949) [25] indicated $y_0 = 0.20k_s$, whereas Grass (1971) [26] found $y_0 = 0.18k_s$. In this study, the reference level is considered as $y_0 = 0.2k_s$, which is in reasonable agreement with the findings of Hinze (1975) [27] and Kironoto & Graf (1994) [28].

The general expression for the logarithmic velocity distribution at the flow depth for hydraulically rough flows can be expressed as follows [28]:

$$\frac{u}{u_*} = \frac{1}{\kappa} \ln\left(\frac{y}{k_s}\right) + B_r \quad (3)$$

where k□ represents the Nikuradse roughness height and B_r is the integration of the numerical constants; B_r = 8.5 for hydraulically rough flows [7, 29, 30].

2.4. Developing Manning's Roughness Coefficient based on Two-point Velocity Measurements

The mean-point velocity for the rough hydraulic flow regime $\left(Re_* = \frac{u_* k_s}{\nu} \geq 70\right)$ can be determined using Equation 4 [21]:

$$\frac{u}{u_*} = 5.75 \log\left(\frac{30y}{k_s}\right) \quad (4)$$

By introducing the definition of Chezy (C) and Darcy–Weisbach (f) as roughness coefficients and integrating Equation 4 over the entire flow depth H, the depth-averaged velocity U_y can be obtained as follows:

$$\frac{\bar{U}_y}{u_*} = \frac{C}{\sqrt{g}} = \sqrt{\frac{8}{f}} = 5.75 \log\left(\frac{12H}{k_s}\right) \quad (5)$$

Equation 4 can be expressed using the velocity measurement data at $y = aH$ and $y = bH$, that is, u_{aH} and u_{bH}, where a and b are constants.

For $y = aH$, (6)

$$\frac{u_{aH}}{u_*} = 5.75 \log\left(\frac{30aH}{k_s}\right) \quad (7)$$

Eliminating u_* from Equations 6 and 7 and defining $\xi = u_{bH}/u_{aH}$, we can obtain:

$$\log\left(\frac{H}{k_s}\right) = \frac{1.477(1-\xi) + \log(b) - \xi\log(a)}{(\xi - 1)} \quad (8)$$

Substituting the $\log\left(\frac{H}{k_s}\right)$ value of Equation 8 into Equation 5,

$$\frac{\bar{U}_y}{u_*} = \frac{C}{\sqrt{g}} = \sqrt{\frac{8}{f}} = 5.75\left(\frac{1.477(1-\xi) + \log(b) - \xi\log(a)}{(\xi - 1)}\right) + 6.21 \quad (9)$$

Substituting Equation 9 into the correlation between the Chezy & Manning roughness coefficients, $n = R^{1/6}/C$, Manning's roughness n at a specific position z/B, where the velocity profiles were measured, can be expressed as [7]:

$$n_{z/B} = \frac{H^{1/6}}{\sqrt{g}\left(\frac{(5.75\log(b) + 2.28) - \xi(2.28 + 5.75\log(a))}{(\xi - 1)}\right)} \quad (10)$$

Equation 10 provides a method for calculating Manning's roughness coefficient, $n_{z/B}$, using the velocity data from two specific points: $y = aH$ and $y = bH$.

The Manning's roughness coefficient for the cross-section, called the composite Manning's roughness coefficient, can then be calculated using the composite Manning's roughness coefficient equation n_{co} as proposed by Lotter (1933) [31]:

$$n_{co} = \frac{PR^{5/3}}{\sum \frac{1}{n_{z/B}} P_{z/B} R_{z/B}^{5/3}} \quad (11)$$

where $P_{z/B}$ and $R_{z/B}$ are the wet perimeter and hydraulic radius for each subarea at *z/B*, respectively; *P* and *R* are respectively the total flow area's wet perimeter and hydraulic radius at a cross-section.

3. Results and Discussion

3.1. Description of Measurement Data

This paper analyzed 1,200 experimental data sets (from 120 flow runs) of velocity profiles and their characteristics under sediment-feeding and non-sediment-feeding flow conditions. In this study, the sediment-feeding flow represented equilibrium sediment transport, whereas the non-sediment-feeding flow corresponded to nonequilibrium sediment transport. The research considered the physical properties of two types of sand and various hydraulic characteristics. Measurements were conducted in both fixed-bed and movable-bed channels, with specific parameters used for identification. Table 1 summarizes the main flow parameter data collected from the measurement results. Given the large amount of data analyzed in this study, not all data can be included in Table 1. More complete and detailed running flow data can be found in Maini (2024) [32].

Table 1. Summary of the main flow parameters for some examples of runs

Run	S_w	H (m)	B/H	R (m)	T (°C)	R_e	F_r	U (m/s)	Q (l/s)	Q_s (kg/s)	$Re_* = u_* k_s/\nu$
Non-sediment feeding flow with fixed bed (NSFFB)											
NSFFBA1-Sand1	0.0015	0.128	4.69	0.090	22.90	351121	0.58	0.651	50	0	72.49
NSFFBA1-Sand2	0.0020	0.119	5.04	0.085	23.20	353570	0.65	0.700	50	0	97.49
…..	….	….	….	….	….	….	….	….	….	….	….
NSFFBO1-Sand1	0.0035	0.121	4.96	0.086	24.10	505346	0.88	0.964	70	0	113.80
NSFFBO1-Sand2	0.0040	0.119	5.04	0.085	23.30	496143	0.91	0.980	70	0	141.46
Sediment feeding flow with fixed bed (SFFB)											
SFFBA1-Sand1	0.0015	0.128	4.69	0.090	23.10	352753	0.58	0.651	50	0.0064	71.19
SFFBA1-Sand2	0.0020	0.119	5.04	0.085	22.70	349492	0.65	0.700	50	0.0049	87.83
…..	….	….	….	….	….	….	….	….	….	….	….
SFFBO1-Sand1	0.0035	0.121	4.96	0.086	21.70	477957	0.88	0.964	70	0.0403	112.08
SFFBO1-Sand2	0.0040	0.119	5.04	0.085	21.30	473457	0.91	0.980	70	0.0264	131.98
Non-sediment feeding flow with movable bed (NSFMB)											
NSFMBA1-Sand1	0.0015	0.134	4.48	0.093	23.10	352753	0.54	0.622	50	0.0235	70.80
NSFMBA1-Sand2	0.0020	0.125	4.79	0.088	23.20	353570	0.60	0.666	50	0.0179	88.23
…..	….	….	….	….	….	….	….	….	….	….	….
NSFMBO1-Sand1	0.0035	0.134	4.48	0.093	22.80	490428	0.76	0.871	70	0.1481	119.82
NSFMBO1-Sand2	0.0040	0.134	4.48	0.093	23.30	496143	0.76	0.871	70	0.0965	134.53
Sediment feeding flow with movable bed (SFMB)											
SFMBA1-Sand1	0.0015	0.131	4.58	0.091	23.70	357668	0.56	0.636	50	0.0294	70.52
SFMBA1-Sand2	0.0020	0.122	4.91	0.087	22.70	349492	0.62	0.682	50	0.0223	83.02
…..	….	….	….	….	….	….	….	….	….	….	….
SFMBO1-Sand1	0.0035	0.128	4.69	0.090	22.30	484742	0.81	0.912	70	0.1852	116.76
SFMBO1-Sand2	0.0040	0.125	4.80	0.088	21.30	473457	0.84	0.934	70	0.1206	142.32

Note: *B*: channel width (= 0.60 m); d_{50}: median diameter of particle (Sand1: uniform sediment = 1.55 mm and Sand2 = 1.85 mm); *U*: cross-section mean velocity ($U = Q/A$); *Q*: flow discharge; Q_s: measured sediment bedload (kg/s); S_w = slope of the water surface; *Re* = Reynolds number; *Fr* = Froude number; *B/H* = aspect ratio width to flow depth; *T* = temperature; Re_* = particle Reynolds number, k_s = the Nikuradse roughness height; *n* = the viscosity of water.

The flow codes were based on the parameters used in the measurement. "SF" denotes sediment-feeding flows, whereas "NSF" stands for non-sediment-feeding flows. "FB" indicates fixed-bed flows, and "MB" signifies movable-bed flows. Letters A to O represent the discharge and channel slope variations, whereas numbers 1 and 2 indicate the

measurement sections 1 m apart. For instance, the code "NSFMBA1-Sand1" indicates that the measurement is from a non-sediment-feeding flow with a movable channel bed, specific discharge, and slope variations, taken from section 1, with bed material referred to as Sand1.

3.2. Velocity Distribution

Figure 4 presents the dimensionless velocity distribution u/U, where u is the point velocity and U is the cross-sectional average velocity. Both flow conditions showed similar trends, with the velocity decreasing near the channel walls due to friction, most notably at vertical positions adjacent to the wall. Additionally, near the channel bottom ($y/H < 0.2$), flows with sediment feeding showed lower u/U values than those without feeding. Specifically, Figure 4-b indicates that sediment transport (fixed bed with sediment feeding) results in lower velocity compared with the non-sediment transport condition in Figure 4-a (fixed bed without sediment feeding), suggesting that sediment transport reduces velocity despite similar flow rates. The position where $u/U = 1$ varies with the transverse position (z/B), typically occurring at $z/B = 0.10–0.20$, indicating that the velocity at this location represents the cross-sectional average velocity. Furthermore, the velocity at $y/H = 0.4$ is generally regarded as the average depth velocity, as supported by Colebrook & White (1937) [33], Keulegan (1938) [19], Maini et al. (2024) [7].

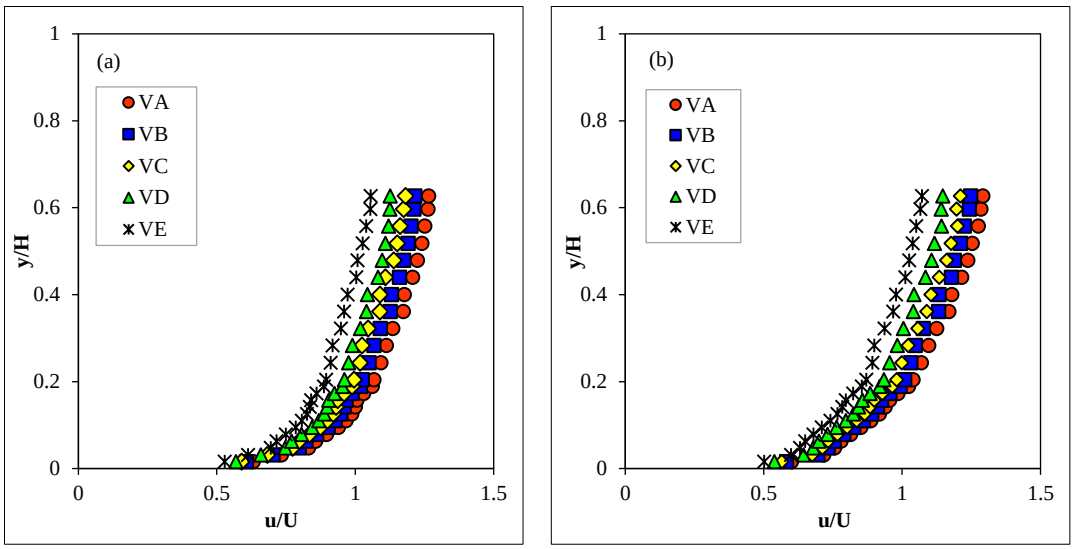

Figure 4. Typical velocity profiles, u/U vs. y/H; Non-sediment feeding fixed-bed (NSFFBA1-Sand1), (b) Sediment feeding fixed-bed (SFFBA1-Sand1)

Figure 5 reveals notable differences in the velocity ratio u/U. In particular, in the inner region ($y/H \leq 0.2$), sediment-fed flows exhibited lower velocities than non-sediment-fed flows. In contrast, the velocity increased in the outer region, as indicated by the arrows in Figure 5. Additionally, the inner region ($y/H \leq 0.2$) displayed a more "slender" velocity profile for sediment-fed flows. A comparison between NSFFBA1 (non-sediment feeding on a fixed bed) and SFFBA1 (sediment feeding on a fixed bed) confirmed this trend, with higher u/U values in NSFFBA1 than in SFFBA1.

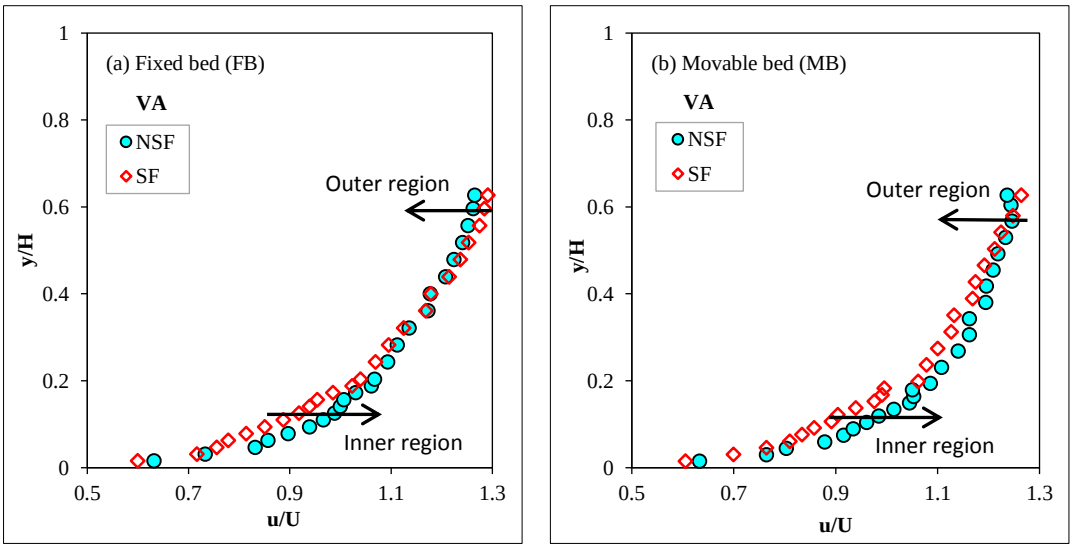

Figure 5. Comparison of the flow velocity distributions between non-sediment feeding and sediment feeding flows: (a) Fixed bed (NSFFBA1-Sand1 and SFFBA1-Sand1); (b) mobile bed (NSFMBA1-Sand1 and SFMBA1-Sand1)

The experimental results also showed that the flow characteristics with sediment feeding for fixed-bed and movable-bed channels differed in the flow velocity distribution in the inner and outer regions ($y/H \leq 0.2$ and $y/H \geq 0.2$). In fixed-bed channels, the flow velocity distribution with sediment feeding in the inner region ($y/H \leq 0.2$) was 16.61% lower than that without sediment feeding. Meanwhile, in movable-bed channels, the flow velocity with sediment feeding in the inner region was 13.16% lower than the flow without sediment feeding.

3.3. Shear Velocity, u_*, and Integration Numeric Constant, Br

The Clauser, energy gradient, and Reynolds stress methods of Kironoto & Graf (1994) [28] can accurately determine the shear velocity. The velocity profiles in log-law coordinates (u_* vs. y/k_s) measured in both fixed-bed and movable-bed channels, with and without sediment feeding, are shown in Figures 6-a, 6-b, 6-c, and 6-d, respectively; the data given in the figures are velocity profile data at the center of the channel. The log-law equation confirms that it adequately explains the data within the inner region [28], with slight deviations occurring in the outer region. The figures show that the measurement data in the inner region follow a logarithmic velocity distribution, allowing for the determination of the shear velocity (and the integration constant B_r) using the Clauser method. This method involves fitting the data from the inner region ($y/H \leq 0.2$), represented in logarithmic coordinates as u versus $\ln(y/k_s)$, to Equation (3), using a least squares adjustment with the Karman constant $\kappa = 0.4$. In the outer region, the velocity profiles slightly deviate from the log-law velocity distribution. This deviation is more pronounced for sediment-feeding flows. There was no significant difference in the velocity profiles for the fixed- and movable-flow data.

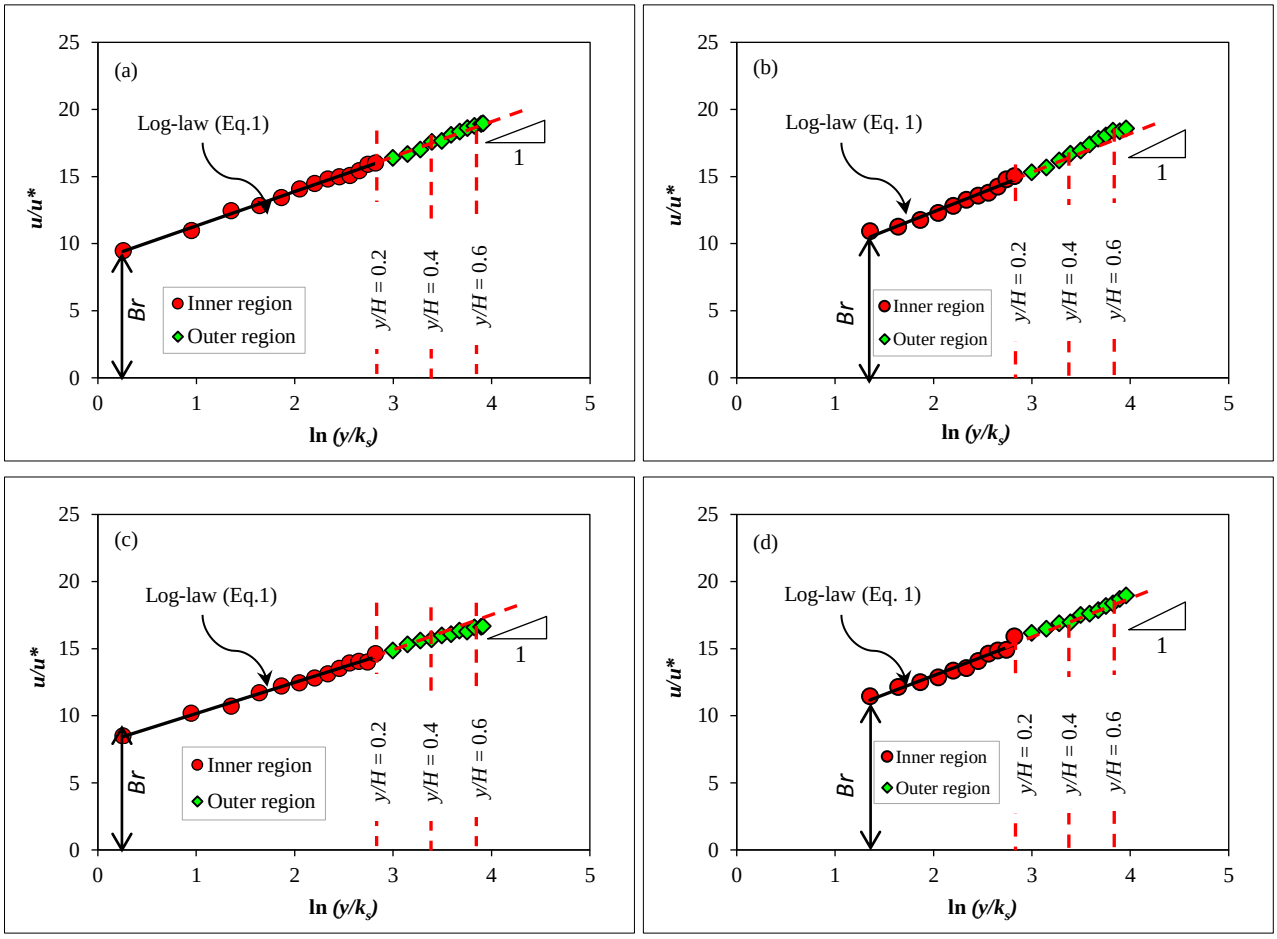

Figure 6. Clauser's method for determining shear velocity (u_*) and integration constant (B_r): (a) Non-sediment feeding with a fixed bed (NSFFBA1-Sand1), (b) sediment feeding with a fixed bed (SFFBA1-Sand1), (c) non-sediment feeding with a movable bed (NSFMBA1-Sand1), and (d) sediment feeding with a movable bed (SFMBA1-Sand1).

In Figure 7, the shear velocity at a given position z/B, normalized by the shear velocity at the center of the channel ($u_{*z/B}/\,u_{*VA}$), is plotted against z/B. The plotted data show that the shear velocity decreases as it approaches the channel walls. The same trend was observed for all the data obtained in this study, that is, for sediment-feeding and non-sediment-feeding flow conditions and fixed and movable beds, even though scattered data were more commonly observed for the plotted data of Sand2, particularly for the data points closer to the channel wall.

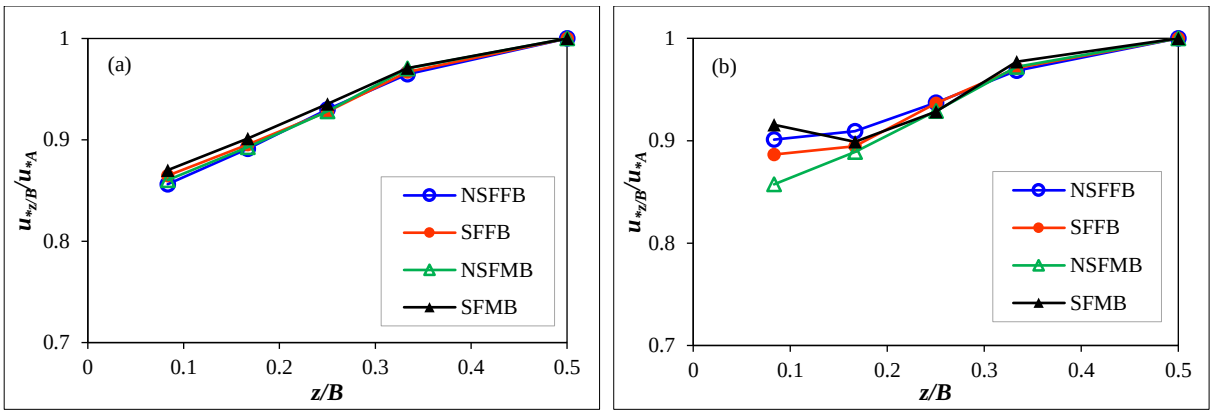

Figure 7. Influence of channel walls on the shear velocity values of the plot of $u_{*z/B}/u_{*VA}$ vs. z/B: (a) Sand1 and (b) Sand2

The plotted data in Figures 8-a and 8-b show the B_r values obtained using the Clauser method at the center of the channel (i.e., at $z/B = 0.5$). For non-sediment-feeding flows, the B_r values were generally around 8.5 ± 15 (as stated by Reynolds (1974, 1979) for clear water flow [34]) and remained relatively constant with $\log(u_* k_s/\nu)$, with the average values of $B_r = 7.57 \pm 0.45$. In contrast, Figure 8-b shows that the B_r values for sediment-feeding flows tended to decrease with $\log (u_* k_s/\nu)$, with some values falling below and outside the range of 8.5 ± 15. There was no significant difference in the *Br* values for the fixed and movable bed flow data and the bed roughness of Sand1 and Sand2

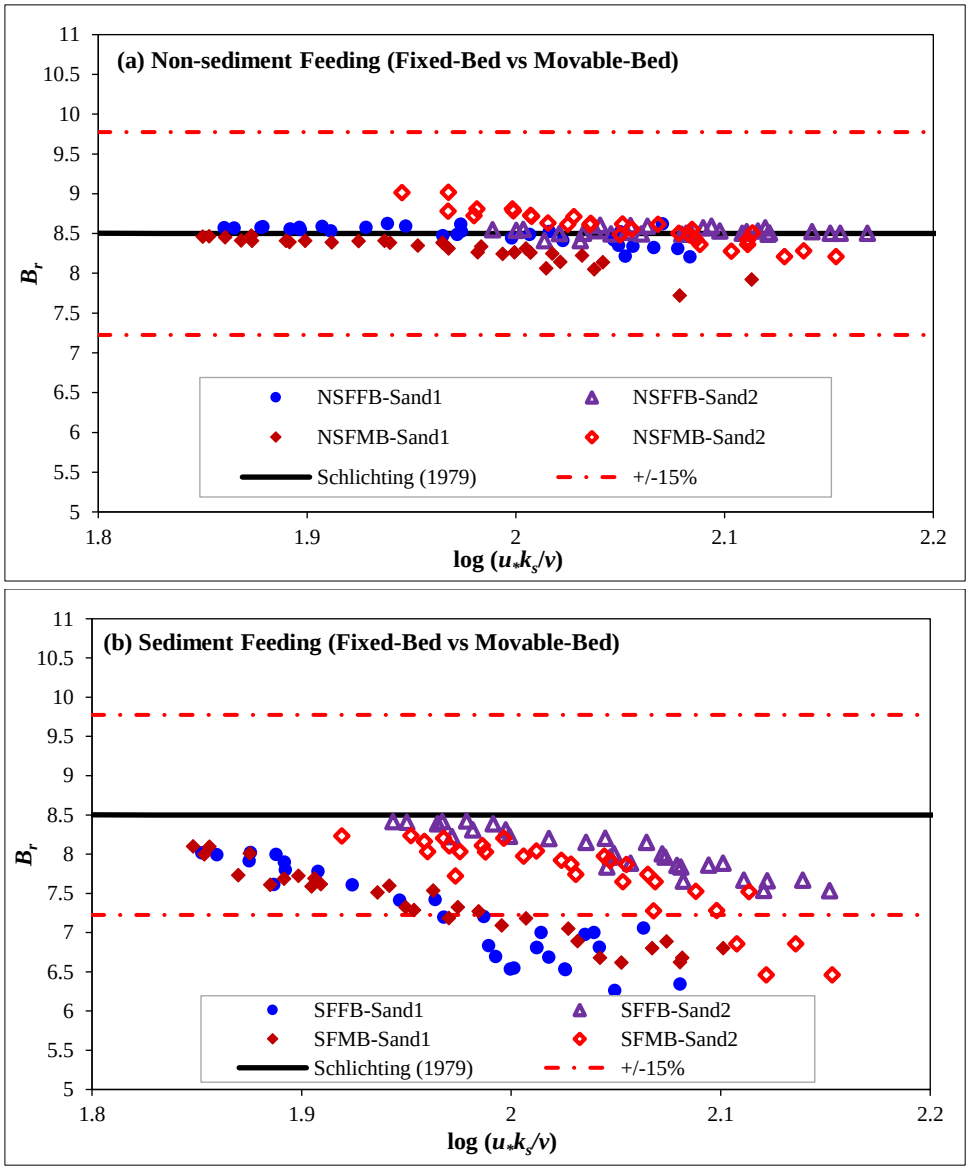

Figure 8. (a) Variation of B_r with roughness Reynolds number $R_{e*} = u_* k_s/\nu$ for non-sediment-feeding flows. (b) Variation of B_r with the roughness particle Reynolds number $R_{e*} = u_* k_s/\nu$ for sediment-feeding flows

In Figure 9, the *Br* values obtained from the Clauser method, using the velocity profile data measured in the inner region at a specific *z/B* position, are plotted against *z/B* in the transverse direction. The B_r values at each *z/B* position in Figure 9 are the average of all data obtained at that specific *z/B*. In the figure, the B_r values are plotted and distinguished based on the sediment-feeding and non-sediment-feeding flow conditions and the fixed-bed and movable-bed conditions. The plot data indicate that the B_r values decrease as they approach the channel wall in the transverse direction, and there is a significant difference in values for the sediment-feeding and non-sediment-feeding flows. Kironoto et al. (2019) [23] observed the same pattern for flow in the field, both in the artificial Mataram irrigation channel and in natural rivers, such as the Kuning River and Opak River in Yogyakarta, Indonesia. Figure 9 also shows that the distinction between the fixed and movable beds is not noticeable.

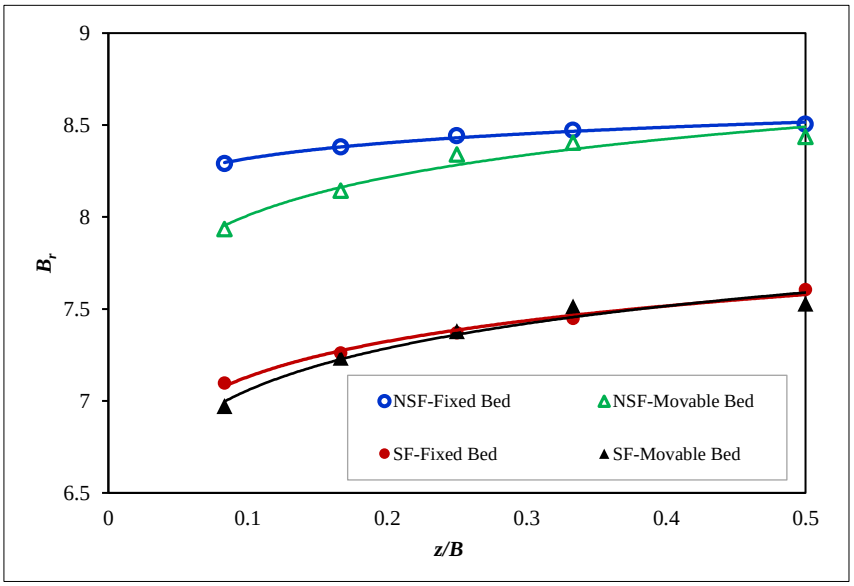

Figure 9. Plot of B_r values vs. *z/B* for non-sediment-feeding and sediment-feeding flows in fixed and movable beds

The plot data in Figure 9 indicate that the B_r value tends to decrease as it approaches the channel sidewall, leading to the derivation of an equation that predicts the B_r value at various vertical positions from the center to the edge of the channel. The regression curves for the B_r value as a function of *z/B* can be derived from the correlation presented in Figure 9. Considering that the differences between the fixed- and movable-bed data are insignificant, the correlation of the B_r value equation as a function of *z/B* is only differentiated for sediment-feeding and non-sediment-feeding flows. The regression curves for B_r as a function of *z/B* can be derived and are given in the following equations.

For non-sediment feeding flow,

$$B_r = 0.21\ln\left(\frac{z}{B}\right) + 8.65 \quad (12)$$

For sediment feeding flow:

$$B_r = 0.30\ln\left(\frac{z}{B}\right) + 7.80 \quad (13)$$

At *z/B* = 0.5, which corresponds to the center of the channel, the B_r values are about 8.5 and 7.6 for the non-sediment-feeding and sediment-feeding flows, respectively.

Thus, on the basis of the laboratory measurement data obtained in this study for both non-sediment-feeding and sediment-feeding flows, the velocity distribution at a specific vertical position in the transverse direction *z/B* can be determined using Equation 3. The B_r values for the non-sediment-feeding and sediment-feeding flows are provided by Equations 12 and 13, respectively. Additional factors that may influence the velocity distribution, such as bed roughness and material gradation, require further verification for laboratory and natural river flows.

3.4. Manning's Roughness Coefficient ($n_{z/B}$) Equation Based on Two-Point Velocity Measurement

In principle, Equation 10 can determine $n_{z/B}$ on the basis of the velocity measurements at two points, *y/H* = *a* and *b*, where *a* and *b* represent any given location of vertical positions at a given depth, as long as the logarithmic law of velocity distribution remains valid throughout the entire flow depth. However, because Equation 10 is derived under the

assumption that the velocity profile follows the logarithmic law, which is theoretically valid in the inner region ($y/H \leq 0.2$), as stated by Nezu & Rodi (1986) [35] and Kironoto & Graf (1994) [28], the use of the two points of y/H in the inner region is preferred. Meanwhile, Keulegan (1938) [19] demonstrated that for practicing purposes, the logarithmic law of velocity distribution can be applied across the entire flow depth, allowing the use of measurement points in the outer region. Given these conditions, Equation 10 for determining $n_{z/B}$ can be evaluated using velocity measurements at two points at any specific y/H location. This applies to the inner and outer regions, provided that the velocity measurements at the two points are accurate and adhere to the logarithmic law.

In this study, these points were taken in the inner and outer regions at the following pairs of points: y/H = 0.1 and 0.2, y/H = 0.2 and 0.4, y/H = 0.2 and 0.6, and y/H = 0.2 and 0.8. Using different pairs of y/H values, specifically y/H = 0.1 and 0.2, y/H = 0.2 and 0.4, y/H = 0.2 and 0.6, and y/H = 0.2 and 0.8, the expression for Equation 10 can be rewritten as Equations 14 to 17, as presented in Table 2.

Table 2. Manning's roughness coefficient equations based on two-point velocity measurements at any point of $y = aH$ and $y = bH$

Two-point velocity measurement at: $y = aH$ and $y = bH$ (u_{aH} and u_{bH})	Manning's roughness coefficient equation	Equation Number
$u_{0.1H}$ and $u_{0.2H}$	$n_{z/B} = \frac{H^{1/6}}{\left[\frac{-5.45 + 10.9\left(\frac{u_{0.2H}}{u_{0.1H}}\right)}{\left(\frac{u_{0.2H}}{u_{0.1H}} - 1\right)}\right]}$	(14)
$u_{0.2H}$ and $u_{0.4H}$	$n_{z/B} = \frac{H^{1/6}}{\left[\frac{-0.03 + 5.45\left(\frac{u_{0.4}}{u_{0.2}}\right)}{\left(\frac{u_{0.4}}{u_{0.2}} - 1\right)}\right]}$	(15)
$u_{0.2H}$ and $u_{0.6H}$	$n_{z/B} = \frac{H^{1/6}}{\left[\frac{3.15 + 5.45\left(\frac{u_{0.6}}{u_{0.2}}\right)}{\left(\frac{u_{0.6}}{u_{0.2}} - 1\right)}\right]}$	(16)
$u_{0.2H}$ and $u_{0.8H}$	$n_{z/B} = \frac{H^{1/6}}{\left[\frac{5.40 + 5.45\left(\frac{u_{0.8}}{u_{0.2}}\right)}{\left(\frac{u_{0.8}}{u_{0.2}} - 1\right)}\right]}$	(17)

On the basis of these pairs of velocity measurements, Equations 14 to 17 can be used to calculate $n_{z/B}$ in the transverse direction z/B. The resulting values of $n_{z/B}$ derived from these equations may vary depending on the quality and accuracy of the velocity measurement data and the degree to which the measured velocity profiles conform to the logarithmic velocity distribution law.

3.5. Composite Manning Roughness Coefficient, n_{co}

The composite Manning's roughness coefficient, n_{co}, was determined using Manning's roughness coefficients at different values of z/B within a cross-section, based on Equations 11 and 10 or their derivative equations, as provided in Table 2. Figure 10 plots n_{co} as a function of the cross-section mean velocity, U, calculated using Equations 11 and 15 for non-sediment-feeding and sediment-feeding flows, respectively. The values range between 0.01 and 0.025. The figure indicates that the n_{co} values for flows with sediment feeding are higher than those without sediment feeding. Comparing the n_{co} values between the bed materials Sand1 (k_s = 1.55 mm) and Sand2 (k_s = 1.85 mm), we observed that Manning's roughness coefficient for Sand2 was higher and more significant than that for Sand1.

In this study, under fixed-bed conditions without sediment transport, Manning's roughness coefficient ranged from 0.010 to 0.017. When sediment was introduced at concentrations between 4.9 and 40.3 g/s, the coefficient increased from 0.013 to 0.022. Under movable-bed conditions, the coefficient increased from 0.019 to 0.025 as the sediment concentration increased to 22.3 and 120.6 g/s. Maini et al. (2024) observed an even more significant increase, with the coefficient reaching between 0.022 and 0.036 for sediment concentrations of 65.1 to 181.5 g/s.

This study also quantified the increases in roughness due to sediment feeding. Compared with clear water flow, sediment transport increased Manning's roughness coefficient by an average of 31.32% in fixed-bed channels and by 27.37% in movable-bed channels. This occurred because the sediment particles reduced the flow velocity and

created a "slender" velocity distribution, resulting in greater roughness (see Figure 5). However, the study was limited to a specific range of sediment concentrations, leaving the effects of higher concentrations unexamined. Further research is needed to determine the upper limits of sediment influence and to enhance our understanding of sediment-laden flow hydraulics.

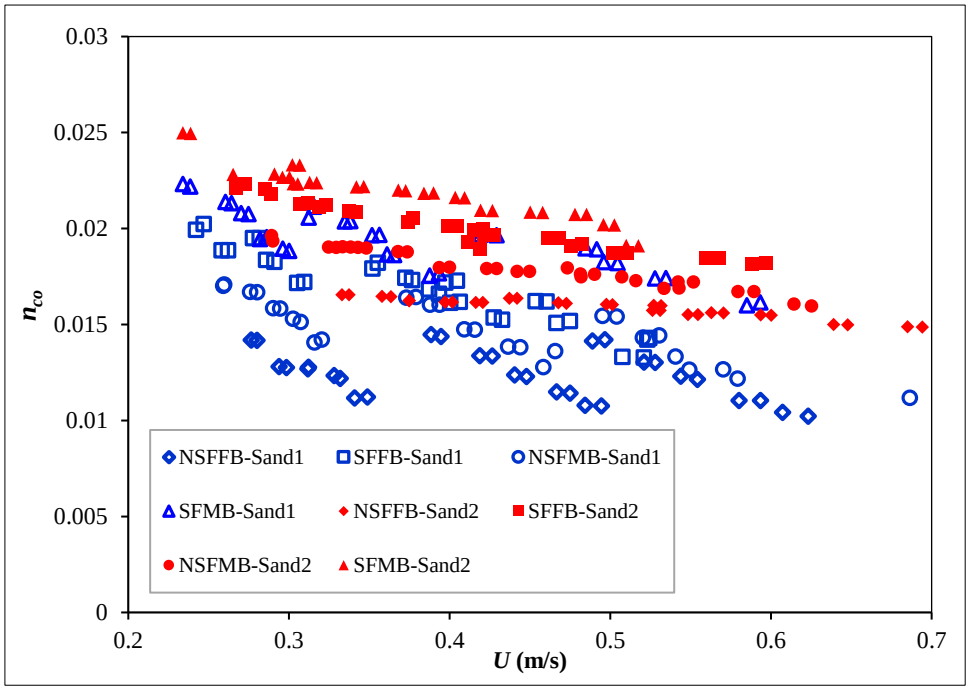

Figure 10. Plot of n_{co} vs. U

3.6. Validation of Manning Roughness Coefficient Equation

For practical purposes, n_{co} (Equation 11) or n (Equation 1) is more practical and valuable compared with $n_{z/B}$ (Equation 10 or its derivative equations in Table 2). Although its calculation is more complex, n_{co}, derived from $n_{z/B}$, is more accurate than n. Furthermore, this equation can also detect the presence of sediment transport on the basis of changes in the velocity profile caused by sediment transport.

The accuracy of n_{co} depends on $n_{z/B}$, which depends on the velocity measurement accuracy. To ensure the validity of Equation 10 or its derivatives (Equations 14 to 17 in Table 2), $n_{z/B}$ was evaluated using two velocity measurement points from 1,200 velocity profiles (from 120 flow runs) measured in this study, covering flows with and without sediment feeding over fixed and movable beds. Additionally, secondary laboratory data obtained by Kironoto (2008) [36] and secondary field data obtained by Kironoto et al. (2018; 2019) [23, 24] were used for further analysis. Kironoto (2008) [36] collected 50 sets of velocity profile data for suspended sediment flow, measured at the Hydraulics and Hydrology Laboratory, Research Center for Engineering Science, Universitas Gadjah Mada in Yogyakarta, Indonesia, covering flows with and without sediment bedload.

Furthermore, 70 sets of velocity profile data from the Mataram irrigation channel in Yogyakarta, Indonesia, collected by Kironoto and Yulistiyanto (2016) [22], 25 sets from the Opak River (Kironoto et al., 2018)[24], and 30 sets from the Kuning River (Yulistiyanto et al., 2019) [23] were included for further analysis. Thus, a total of 225 secondary velocity profile datasets were used as supplementary data to verify and validate the Manning's roughness coefficient equations.

Composite Manning's roughness coefficients n_{co} obtained from Manning's roughness coefficient at z/B and at specific positions of y/H, namely, n_{co} (y/H), calculated using Equation 11 together with Equations 14 to 17, were compared with each other and plotted in Figures 11-a to 11-c. In Figure 11-c, because of the limitations of the ADV equipment used in this study, which could not measure the velocity at y/H = 0.8, the n_{co} values based on $n_{z/B}$ for y/H = 0.2 and 0.8 were not included.

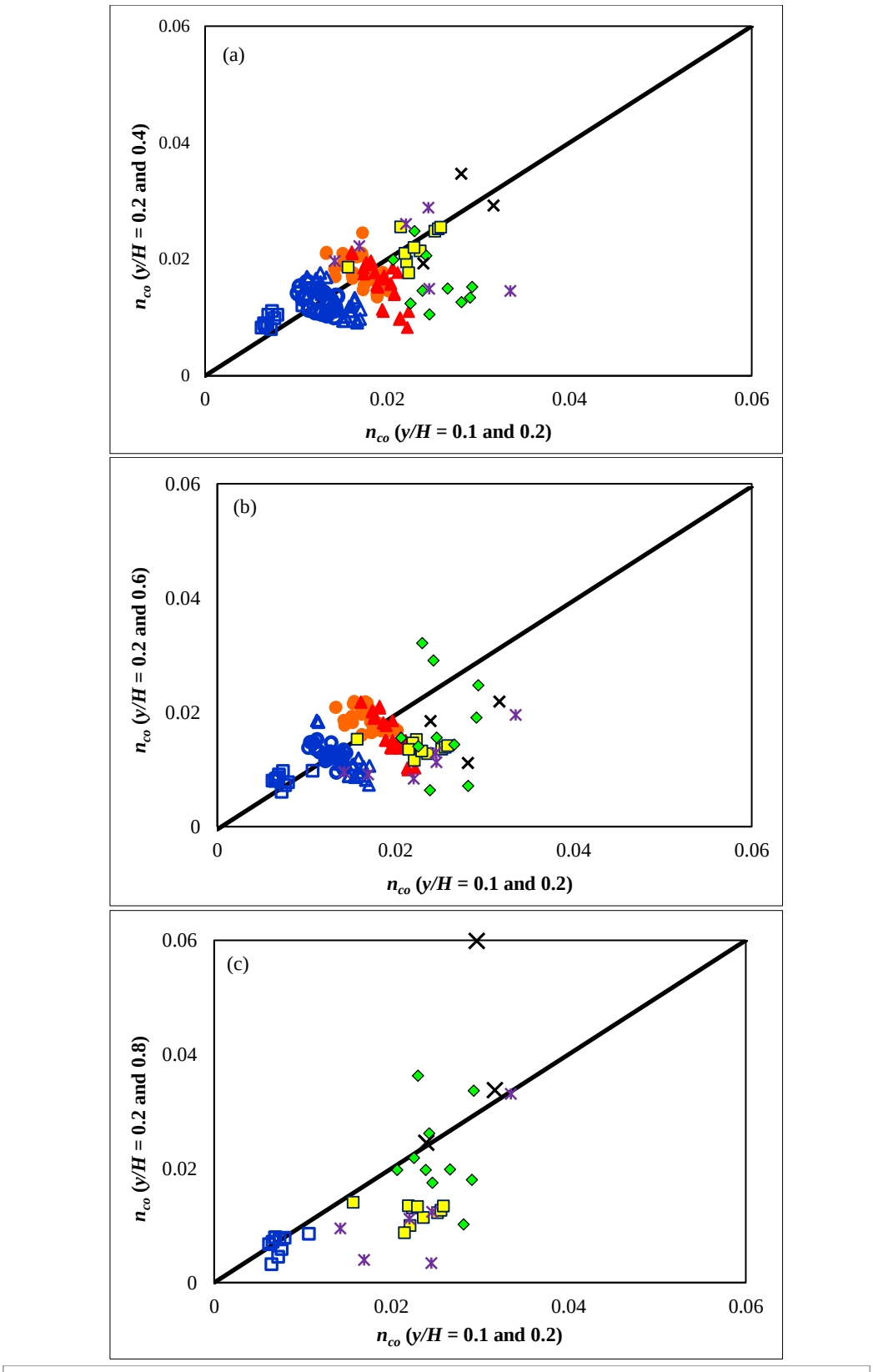

Figure 11. Comparison of n_{co} (y/H) values based on the two-point velocity at (a) y/H = 0.1 and 0.2 vs y/H = 0.2 and 0.4, (b) y/H = 0.1 and 0.2 vs y/H = 0.2 and 0.6, and (c) y/H = 0.1 and 0.2 vs. y/H = 0.2 and 0.8

The data plotted in Figures 11-a to 11-c show that when n_{co} calculated using Equations 10 and 14—for y/H = 0.1 and 0.2—was set as the reference value and compared with the values calculated using the three other equations (Equations 15, 16, and 17), the comparison showed a poor match, especially for the field data, either for irrigation channel or natural river data. This discrepancy was most likely caused by the challenges and potential inaccuracies associated with the flow velocity measurements in the inner region, even though the velocity measurement data in this region ($y/H \leq 0.2$) should be more favorable as they followed the logarithmic law of velocity distribution [28].

The comparison of n_{co} values illustrated in Figures 11-a to 11-c shows that n_{co} calculated using $n_{z/B}$ with velocity data from points at y/H = 0.1 and 0.2 produced different results compared with those derived from other pairs of points of y/H, such as y/H = 0.2 and 0.4, y/H = 0.2 and 0.6, or y/H = 0.2 and 0.8. Consequently, it was not possible to definitively conclude which position of y/H offers the most accurate prediction of n_{co}. Considering the inadequacy of the comparison results in Figures 11-a to 11-c, we must determine which pair of y/H provides n_{co} values closest to each other or offers the best prediction of n_{co}. To achieve this, calculations and comparisons were performed using the same methods and equations described earlier. After conducting several calculations and comparisons, n_{co} determined using $n_{z/B}$ with the paired values of y/H = 0.2 and 0.4 (Equation 15) had the best agreement with n_{co} calculated using other paired y/H-values. Figure 12 compares the n_{co} values calculated using Equation 15 (y/H = 0.2 and 0.4) and Equation 16 (y/H = 0.2 and 0.6). These positions lay in the region around the inner and outer regions. Notably, most velocity profile data within the $0.2 \leq y/H \leq 0.60$ range closely aligned with the logarithmic velocity distribution law, especially for the present laboratory data (see Figure 6 above). Therefore, calculating $n_{z/B}$ within this position range can provide reasonable predictions of $n_{z/B}$. The data quality within this range is likely more reliable as the potential difficulties in velocity measurement are relatively less challenging than those in the inner region ($y/H \leq 0.2$). For the field data, scattering was observed, which might also be related to measurement data difficulties and was more challenging than that of the laboratory measurements.

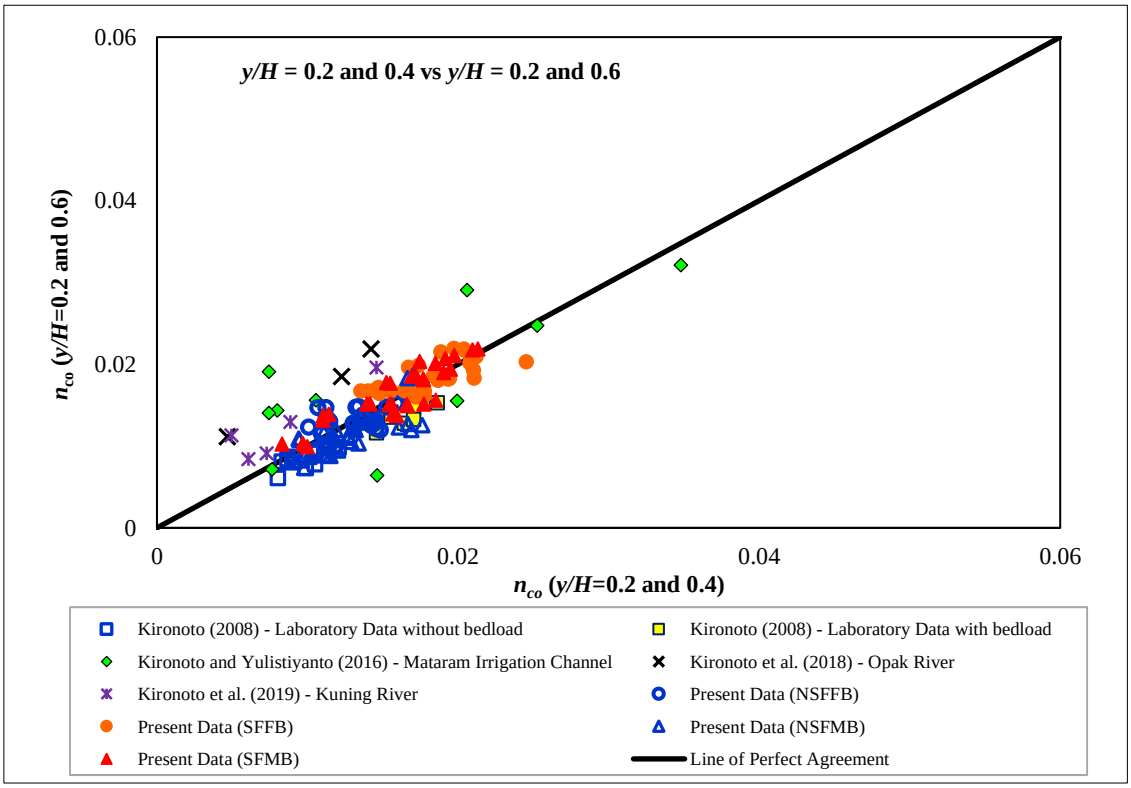

Figure 12. Comparison of n_{co} values determined using $n_{z/B}$ with the two points of velocity at y/H = 0.2 and 0.4 and at y/H = 0.2 and 0.6

For $y/H > 0.6$, some measurement data showed deviations from the logarithmic velocity distribution, following the velocity distribution law in the wake zone [28]. Consequently, the pair values of y/H = 0.2 and 0.8 did not give better results than those of the pair points y/H = 0.2 and 0.4. In conclusion, given the above-analyzed data, n_{co} can be determined using $n_{z/B}$ with velocity data taken from paired points of y/H = 0.2 and 0.4.

In addition to n_{co}, n, as given in Equation 1, is often used for practical purposes. A study and comparison assessed how well the composite Manning's roughness coefficient values calculated using Equations 11 and 15 align with those calculated using Equation 1. The plot of n_{co} and n for flow data with SF and NSF of the present data is shown in Figure 13. The data fell close to the line of perfect agreement, indicating that n_{co}, calculated using Equation 11 together with Equation 15, and n, calculated using Equation 1, provided nearly identical predictions, particularly for the data without

sediment feeding. However, for the data with sediment feeding, it could be observed that n_{co} was greater than n because n_{co} incorporated velocity distribution data, whose distribution shape was known to change due to sediment feeding (bed load). In contrast, Equation 1, which was used to calculate n, could not account for the presence or absence of sediment-feeding effects.

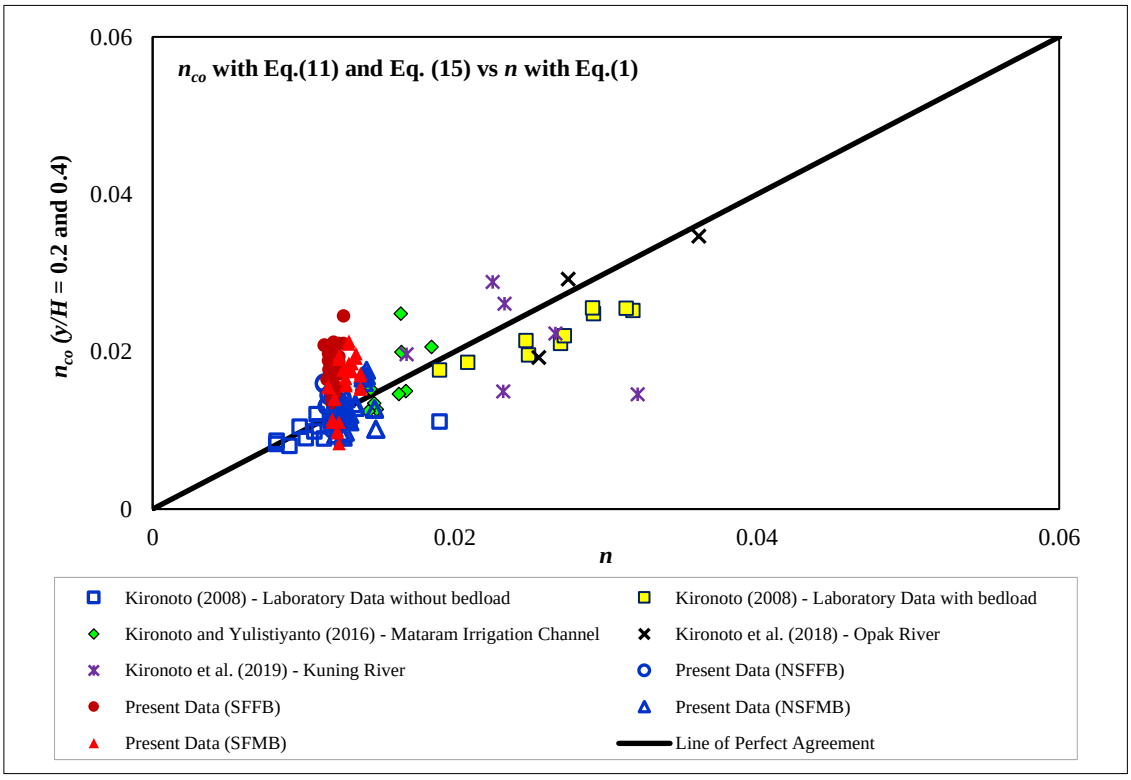

Figure 13. Plot of n_{co} using two points of velocity at y/H = 0.2 and 0.4 vs. n

Many significant scattered data were observed for the field measurements, likely due to challenges and potential inaccuracies in the flow velocity measurements. Another factor that may have contributed to the data scatter was the influence of suspended sediment (and bed load sediment) on the velocity profile (Kironoto, 2008) [36]. These factors influenced the composite Manning's roughness coefficient, which was determined from two-point velocities. However, their impact on the velocity distribution, including their effect on n_{co}, could not be thoroughly evaluated in this study. Conversely, n remained unchanged despite the sediment transport.

n_{co}, calculated using Equations 11 and 15, was generally higher than n obtained from Equation 1, particularly for sediment-feeding flows (see Figure 13). The differences reached 33.01% for the fixed bed and 36.52% for the movable bed. The difference was smaller for non-sediment-feeding flows, with increases of 14.80% for the fixed bed and 18.17% for the movable bed. Despite these variations, the values remained within the acceptable limits for practical applications. The higher n_{co} can be attributed to the physical processes occurring within the flow. The composite Manning approach considers velocity variations across vertical subareas within a single cross-section, providing a more accurate representation of flow inhomogeneity. In contrast, cross-sectional methods rely on a cross-sectional average, which does not fully capture the detailed velocity distribution.

The increase in Manning's roughness coefficient caused by flows carrying sediment particles suggests that sediment-feeding flows likely consume more energy and result in more significant energy losses as a substantial amount of energy is expended in lifting and transporting sediment particles, as stated by Chow (1959) [1], Song et al. (1998) [12], Maini et al. (2023) [37], and Maini et al. (2024) [7, 38].

3.7. Determination of Composite Manning Roughness Coefficient, n_{co}, as a function of z/B

As previously mentioned, the calculation of the composite Manning's roughness coefficient using Equations 11 and 15 requires velocity data at several transverse positions (z/B) within a cross-section and at specific vertical positions (y/H). This process can be quite time-consuming. Therefore, a method is needed where the required velocity measurement data are limited to particular z/B positions only. While the y/H positions have been discussed and proposed, such as at y/H = 0.2 and 0.4, the evaluation of $n_{z/B}/n_{co}$ as a function of z/B is presented in the following.

Figure 14 shows the plot of $n_{z/B}/n_{co}$ as a function of z/B in the transverse direction, where $n_{z/B}$ represents Manning's roughness coefficient at z/B and n_{co} is the composite Manning's roughness coefficient for the section. The regression

curve presented in the figure is based on the laboratory data obtained in this study. The curve in the figure indicates that the $n_{z/B}/n_{co}$ values for the present data tend to decrease as they approach the channel sidewall. It is also observed with small data scatter that the point where $n_{z/B}/n_{co} = 1$ occurs at $z/B = 0.2$. This suggests that $n_{z/B}$ measured at $z/B = 0.2$ from the channel sidewall provides a good representation of n_{co} for the section. Although this assumption may be sensitive to variations in channel cross-sectional shape and width-to-depth ratio, the present laboratory data — characterized by rectangular cross-sections and B/H ratios between 3.85 and 6 — did not exhibit significant sensitivity, as the variation remained within an acceptable scatter range.

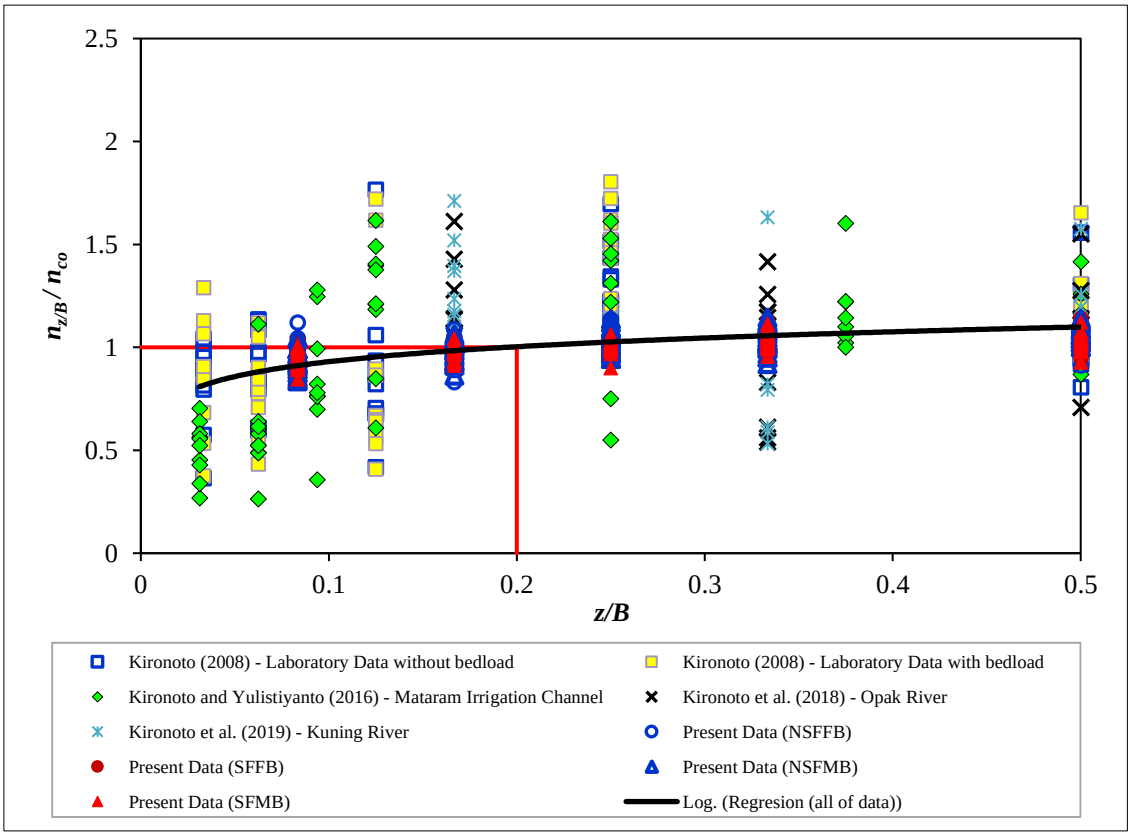

Figure 14. The plot of Manning roughness coefficient $n_{z/B}/n_{co}$ vs. z/B

The same figure also includes secondary data from Kironoto (2008) [36], Kironoto & Yulistiyanto (2016) [22], and Kironoto et al. (2018, 2019) [23, 24]. In contrast, the field data displayed greater scatter, likely due to more irregular channel cross-sections and wider variability in width-to-depth ratios. For instance, the Mataram irrigation channel has a trapezoidal cross-section, while the Opak and Kuning Rivers exhibit natural, irregular cross-sections, differing substantially from the rectangular sections used in the laboratory experiments. Therefore, further research is recommended to evaluate the validity of this assumption under more complex and variable channel geometries.

After evaluating the plot data in Figures 13 and 14, it can be suggested that n_{co} can be determined using velocity measurement data at depths of $y/H = 0.2$ and 0.4 and at a transverse position of $z/B = 0.20$ from the channel sidewall.

3.8. Comparison of Manning's Roughness Coefficients in the Present and Previous Studies

Figure 15 compares Manning's roughness coefficients from this study with those of previous research by Boyer (1954) [39], Zhang et al. (2010) [8], and Maini et al. (2024) [7], along with the previously mentioned secondary data. The present study included experimental results under fixed-bed and movable-bed conditions, both with and without sediment transport. Meanwhile, Boyer (1954) [39] analyzed velocity distribution data from 22 natural rivers in the northwestern United States, reporting H/k_s values ranging from 1.3 to 220, with most values below 20. Boyer (1954) [39] estimated Manning's roughness coefficient based on the velocity at points $y/H = 0.2$ and $y/H = 0.8$ to determine the cross-sectional Manning's roughness coefficient and did not calculate the composite Manning's roughness coefficient. Zhang et al. (2010) [8] estimated Manning's roughness coefficient using the average cross-sectional velocity, obtaining H/k_s values below 40. This study recorded H/k_s values above 50, whereas Maini et al. (2024) [7] reported values exceeding 100. Except for some data from Zhang et al. (2010) [8], all the plotted data fell within a similar $n/H^{1/6}$ range and followed a consistent trend: Manning's roughness coefficient (n) decreased as the H/k_s values increased. This indicates that in deeper flows, bed roughness has less influence on the velocity near the surface, resulting in lower roughness values.

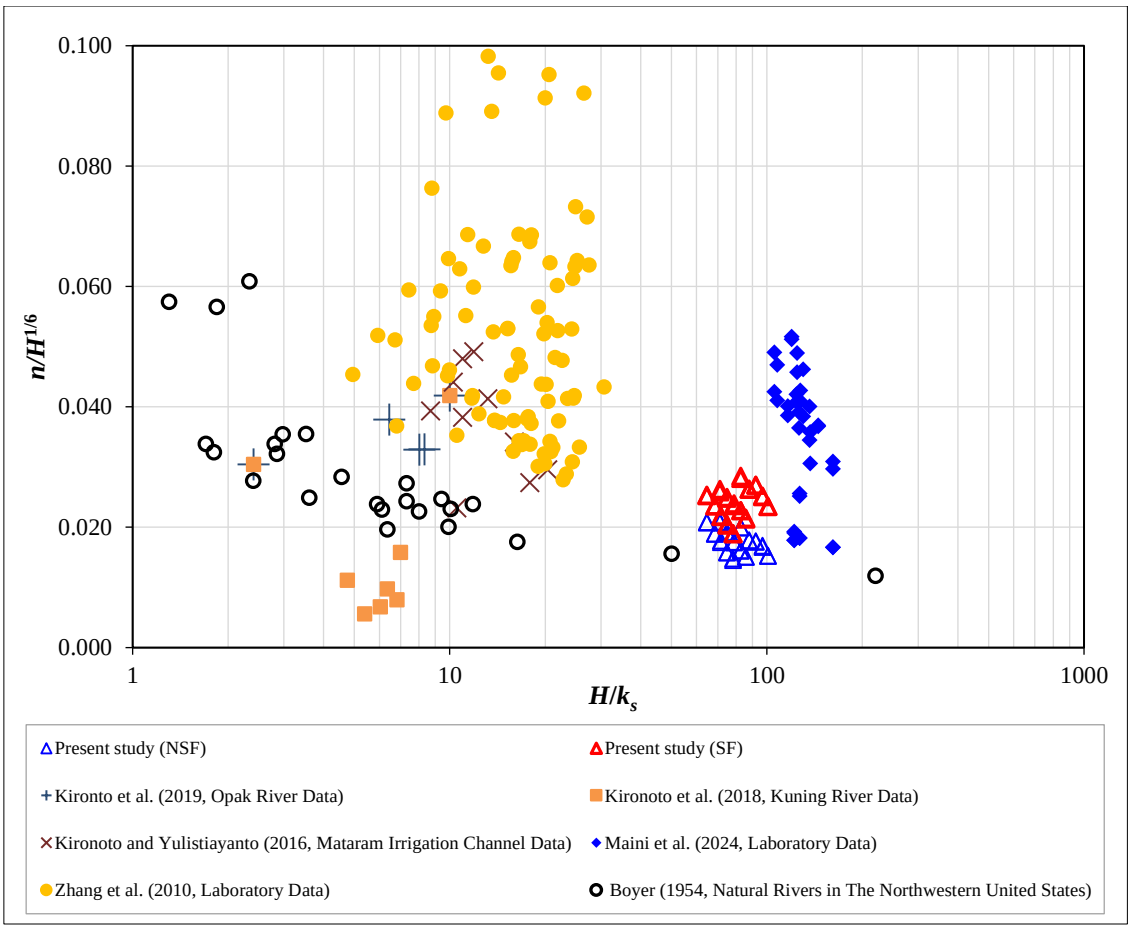

Figure 15. Comparison of Manning's roughness coefficients in the present and previous studies

4. Conclusions

This study takes an alternative approach by using two points of velocity profiles to examine how sediment feeding affects Manning's roughness coefficient. After analyzing the velocity data profiles of primary and secondary data sets, some findings are drawn as follows.

- In sediment-feeding flows, particularly in inner regions ($y/H \leq 0.2$), the flow velocity (u/U) is lower than that in non-sediment-feeding flows. However, farther from the wall, the velocity in sediment-feeding flows is relatively higher than that in non-sediment-feeding flows. This change in the velocity profile, especially in inner regions, impacts the shear velocity u_* and the logarithmic velocity distribution law's numerical integration constant Br.
- The B_r value obtained using the Clauser method decreases as it approaches the channel sidewall; non-sediment-feeding flows have higher B_r values than sediment-feeding flows; that is, $B_r = 8.5 \pm 15\%$. Meanwhile, the B_r value in flows with sediment feeding tends to be smaller (less than 8.5), where some values fall below and outside the range of $8.5 \pm 15\%$.
- $n_{z/B}$ in the transverse direction can be determined using two points of the velocity profile at z/B, with $y/H = 0.2$ and 0.4, according to Equation (15). The differences in the shape of the velocity profiles (u/U) due to sediment feeding, particularly in the inner region ($y/H \leq 0.2$), affect the value of $n_{z/B}$.
- n_{co} can be determined from $n_{z/B}$ using Equations (11) and (15). The values of n_{co} are generally higher than n obtained from Equation (1), particularly for sediment-feeding flows.
- In the case of non-sediment-feeding flow, the differences in n_{co} compared with n are 14.80% for a fixed bed and 18.17% for a movable bed. These differences are more pronounced for sediment-feeding flow at 33.01% for a fixed bed and 36.52% for a movable bed. In addition, the n_{co} value for sediment-feeding flows tends to be higher than the n_{co} value for non-sediment-feeding flows.
- The point where $n_{z/B}/n_{co} = 1$ occurs at $z/B = 0.2$ from the channel sidewall, which suggests that $n_{z/B}$ measured at $z/B = 0.2$ from the channel sidewall provides a good representation of n_{co} for the section.
- The Manning roughness coefficient, n, decreases as H/k_s increases, as deeper flows reduce the influence of bed roughness. This trend is consistent with previous studies compared with the present data.

5. Declarations

5.1. Author Contributions

Conceptualization, B.A.K. and M.M.; methodology, M.M.; software, I.I.; validation, B.A.K., A.P.R., and I.I.; formal analysis, M.M.; investigation, M.M. and B.A.K; resources, I.I.; data curation, A.P.R.; writing—original draft preparation, M.M. and B.A.K.; writing—review and editing, M.M., B.A.K., A.P.R., and I.I; visualization, I.I.; supervision, B.A.K.; project administration, B.A.K. and M.M.; funding acquisition, A.P.R. All authors have read and agreed to the published version of the manuscript.

5.2. Data Availability Statement

The data presented in this study are available in the article.

5.3. Funding

The author received financial support from the Final Project Recognition Grant ("Program Rekognisi Tugas Akhir Tahun 2024"), Universitas Gadjah Mada, based on Decree Number: 370/UN1.P1/KPT/HUKOR/2024 dated 3 May 2024 and Letter of Assignment Number 5286/UN1.P1/PT.01.03/2024 dated 6 May 2024, provided by the Research Directorate of Universitas Gadjah Mada for this research, authorship, and publication of this article.

5.4. Acknowledgements

The authors wish to acknowledge the Final Project Recognition Grant ("Program Rekognisi Tugas Akhir Tahun 2024") from Universitas Gadjah Mada, based on Decree Number 370/UN1.P1/KPT/HUKOR/2024 dated 3 May 2024 and Letter of Assignment Number: 5286/UN1.P1/PT.01.03/2024 dated 6 May 2024, provided by the Research Directorate of Universitas Gadjah Mada for funding. The authors also thank the Hydraulics and Hydrology Laboratory, Research Center for Engineering Science, Universitas Gadjah Mada, Yogyakarta, Indonesia, for providing the recirculating sediment flume.

5.5. Conflicts of Interest

The authors declare no conflict of interest.

6. References

[1] Chow, V. T. (1960). Open-Channel Hydraulics. Ven Te Chow. McGraw-Hill, New York, United States.

[2] W. L. Cowan. (1956). Estimating hydraulic roughness coefficients. Agricultural Engineering, 37(7), 473–475.

[3] Arcement, G. J., & Schneider, V. R. (1989). Guide for selecting Manning's roughness coefficients for natural channels and flood plains (No. 2339). USGPO; For sale by the Books and Open-File Reports Section, US Geological Survey, Reston, United States. doi 10.3133/wsp2339.

[4] Allen, T. G. (2014). A Study of the Variability Versus the Assumed Constancy of Manning's n. Ph.D. Thesis, Utah State University, Logan, United States.

[5] Rad, H. R., Ebrahimian, H., Liaghat, A., Khalaji, F., & Arani, M. S. (2025). Temporal variation of Manning roughness coefficient in furrow irrigation and its relationship with various field parameters. Applied Water Science, 15(1), 7. doi:10.1007/s13201-024-02334-9.

[6] Julien, P. Y. (2016). Gradually Varied Flow. Essentials of hydraulics. Cambridge University Press, Cambridge, United Kingdom. doi:10.1017/9781108907446.011.

[7] Maini, M., Kironoto, B. A., Istiarto, & Rahardjo, A. P. (2024). Evaluating Manning's Roughness Coefficient for Flows with Equilibrium and Non-equilibrium Sediment Transport. Jordan Journal of Civil Engineering, 18(1), 65–80. doi:10.14525/JJCE.v18i1.06.

[8] Zhang, G. H., Luo, R. T., Cao, Y., Shen, R. C., & Zhang, X. C. (2010). Impacts of sediment load on Manning coefficient in supercritical shallow flow on steep slopes. Hydrological Processes, 24(26), 3909–3914. doi:10.1002/hyp.7892.

[9] Gao, P., & Abrahams, A. D. (2004). Bedload transport resistance in rough open-channel flows. Earth Surface Processes and Landforms, 29(4), 423–435. doi:10.1002/esp.1038.

[10] Campbell, L., McEwan, I., Nikora, V., Pokrajac, D., Gallagher, M., & Manes, C. (2005). Bed-Load Effects on Hydrodynamics of Rough-Bed Open-Channel Flows. Journal of Hydraulic Engineering, 131(7), 576–585. doi:10.1061/(asce)0733-9429(2005)131:7(576).

[11] Bergeron, N. E., & Carbonneau, P. (1999). The effect of sediment concentration on bedload roughness. Hydrological Processes, 13(16), 2583-2589. doi:10.1002/(sici)1099-1085(199911)13:16<2583::aid-hyp939>3.0.co;2-s.

[12] Song, T., Chiew, Y. M., & Chin, C. O. (1998). Effect of Bed-Load Movement on Flow Friction Factor. Journal of Hydraulic Engineering, 124(2), 165–175. doi:10.1061/(asce)0733-9429(1998)124:2(165).

[13] Smart, G. M., & Jaeggi, M. N. R. (1983). Sediment transport on steep slopes. Communications from the Research Institute for Hydraulic Engineering, Hydrology and Glaciology, 64, 91-191.

[14] Nikora, V. I., & Smart, G. M. (1997). Turbulence Characteristics of New Zealand Gravel-Bed Rivers. Journal of Hydraulic Engineering, 123(9), 764–773. doi:10.1061/(asce)0733-9429(1997)123:9(764).

[15] Carbonneau, P. E., & Bergeron, N. E. (2000). The effect of bedload transport on mean and turbulent flow properties. Geomorphology, 35(3–4), 267–278. doi:10.1016/S0169-555X(00)00046-5.

[16] Zhang, K., Li, N., Fu, S., Mu, H., & Lu, B. (2025). The mechanism of surface cover influences the sediment transport capacity. Journal of Hydrology, 651, 132527. doi:10.1016/j.jhydrol.2024.132527.

[17] Hou, L., & Zhang, H. (2025). Research on the calculation method of frictional resistance in the lower reaches of the Yellow River. Shuili Xuebao/Journal of Hydraulic Engineering, 56(1), 63–72. doi:10.13243/j.cnki.slxb.20240170.

[18] Manning, R. (1891). On the flow of water in open channels and pipes. Transactions, Institution of Civil Engineers of Ireland, 20, 161.

[19] Keulegan, G. H. (1938). Laws of turbulent flow in open channels. Journal of Research of the National Bureau of Standards, 21(6), 707. doi:10.6028/jres.021.039.

[20] Woo, H. S., Julien, P. Y., & Richardson, E. V. (1988). Suspension of Large Concentrations of Sands. Journal of Hydraulic Engineering, 114(8), 888–898. doi:10.1061/(asce)0733-9429(1988)114:8(888).

[21] Van Rijn, L.C. (1993) Principles of Sediment Transport in Rivers, Estuaries and Coastal Areas. Aqua Publications, Amsterdam, Netherelands.

[22] Kironoto, B. A., & Yulistiyanto, B. (2016). The simplified of suspended sediment measurement method for predicting suspended sediment load as a basic of reservoir capacity design as renewable energy resource. International Journal of Renewable Energy Research, 6(1), 315–322. doi:10.20508/ijrer.v6i1.3026.g6788.

[23] Yulistiyanto, B., Kironoto, B., Giarto, B., Kiptiah, M., & Tantowi, M. L. (2019). The Simplified of Suspended Sediment Measurement Method in Natural River (Case study of Kuning River in Yogyakarta, Indonesia). Journal of the Civil Engineering Forum, 5(3), 243. doi:10.22146/jcef.47061.

[24] Kironoto, B. A., Yulistiyanto, B., Giarto, R. B., Kiptiah, M., & Sitinjak, O. E. (2018). The simplified of suspended sediment measurement method for predicting suspended sediment discharge in natural river (case study of Opak River, Yogyakarta, Indonesia). Proceedings - International Association for Hydro-Environment Engineering and Research (IAHR)-Asia Pacific Division (APD) Congress: Multi-Perspective Water for Sustainable Development, IAHR-APD 2018, 1, 273–281.

[25] Einstein, H. A., & El-Samni, E. S. A. (1949). Hydrodynamic forces on a rough wall. Reviews of Modern Physics, 21(3), 520–524. doi:10.1103/RevModPhys.21.520.

[26] Grass, A. J. (1971). Structural features of turbulent flow over smooth and rough boundaries. Journal of Fluid Mechanics, 50(2), 233–255. doi:10.1017/S0022112071002556.

[27] Hinze, J. O. (1959). Turbulence. McGraw-Hill, New York, United States.

[28] Kironoto, B. A., & Graf, W. H. (1994). Turbulence characteristics in rough uniform open-channel flow. Proceedings of the Institution of Civil Engineers: Water, Maritime and Energy, 106(4), 333–344. doi:10.1680/iwtme.1994.27234.

[29] Schlichting, H. (1979) Boundary Layer Theory. 7th Edition, McGraw-Hill, New York, United States. doi:10.1115/1.3240614.

[30] Schlichting, H., & Gersten, K. (2016). Boundary-layer theory. Springer-Verlag, Berlin, Germany. doi:10.1007/978-3-662-52919-5.

[31] Lotter, G. K. (1933). Considerations on hydraulic design of channels with different roughness of walls. Transactions, All-Union Scientific Research Institute of Hydraulic Engineering, Leningrad, 9, 238-241.

[32] Maini, M. (2024). The Effect of Sediment Transport on Manning's Roughness Coefficient in Open Channels. Ph.D. Thesis, Yogyakarta, Indonesia.

[33] Colebrook, C. F., & White, C. M. (1937). the Reduction of Carrying Capacity of Pipes with Age. Journal of the Institution of Civil Engineers, 7(1), 99–118. doi:10.1680/ijoti.1937.14682.

[34] Reynolds, A. J. (1974). Turbulent flows in engineering. John Wiley & Sons, Hoboken, United States.

[35] Nezu, I., & Rodi, W. (1986). Open- channel Flow Measurements with a Laser Doppler Anemometer. Journal of Hydraulic Engineering, 112(5), 335–355. doi:10.1061/(asce)0733-9429(1986)112:5(335).

[36] Kironoto, B. A. (2008). verage suspended sediment concentration at depth based on 1, 2, and 3 point measurements in open channel uniform flow. Dinamika Teknik Sipil, 8(1), 59-71. (In Indonesian).

[37] Maini, M., Kironoto, B. A., Rahardjo, A. P., & Istiarto. (2023). Flow Characteristics of Equilibrium and Non-Equilibrium Sediment Transport Flows. International Journal of GEOMATE, 25(110), 77–86. doi:10.21660/2023.110.3957.

[38] Maini, M., Kironoto, B. A., Rahardjo, A. P., & Istiarto. (2024). Effect of equilibrium and non-equilibrium sediment transport flows on the shear velocity in an open channel. IOP Conference Series: Earth and Environmental Science. doi:10.1088/1755-1315/1311/1/012013.

[39] Boyer, M. C. (1954). Estimating the Manning coefficient from an average bed roughness in open channels. Eos, Transactions American Geophysical Union, 35(6), 957-961. doi:10.1029/TR035i006p00957.